Deletions and Point Mutations of *LRRC50* Cause Primary Ciliary Dyskinesia Due to Dynein Arm Defects

Niki Tomas Loges,[1,2,13,14] Heike Olbrich,[1,13,14] Anita Becker-Heck,[1,2] Karsten Häffner,[1] Angelina Heer,[1] Christina Reinhard,[1] Miriam Schmidts,[1] Andreas Kispert,[3] Maimoona A. Zariwala,[4] Margaret W. Leigh,[5] Michael R. Knowles,[6] Hanswalter Zentgraf,[7] Horst Seithe,[8] Gudrun Nürnberg,[9] Peter Nürnberg,[9,10,11] Richard Reinhardt,[12] and Heymut Omran[1,13,*]

Genetic defects affecting motility of cilia and flagella cause chronic destructive airway disease, randomization of left-right body asymmetry, and, frequently, male infertility in primary ciliary dyskinesia (PCD). The most frequent defects involve outer and inner dynein arms (ODAs and IDAs) that are large multiprotein complexes responsible for cilia-beat generation and regulation, respectively. Here, we demonstrate that large genomic deletions, as well as point mutations involving *LRRC50*, are responsible for a distinct PCD variant that is characterized by a combined defect involving assembly of the ODAs and IDAs. Functional analyses showed that LRRC50 deficiency disrupts assembly of distally and proximally DNAH5- and DNAI2-containing ODA complexes, as well as DNALI1-containing IDA complexes, resulting in immotile cilia. On the basis of these findings, we assume that LRRC50 plays a role in assembly of distinct dynein-arm complexes.

Motility of cilia and flagella plays a role in diverse biological processes during embryogenesis and maintenance of organ integrity.[1] Monocilia at the embryonic node generate an extraembryonic fluid flow, which is required for determination of embryonic left-right asymmetry.[2] Motility of multiple cilia lining respiratory epithelial cells is responsible for mucociliary clearance. Analogously, ependymal cilia mediate cerebrospinal fluid flow through the Sylvian aqueduct.[3] Furthermore, flagellar motility is required for sperm cells to propel through the female reproductive system.

Most of the genetically characterized primary ciliary dyskinesia (PCD [MIM 242650]) variants exhibit mutations in genes (*DNAH5* [MIM 603335]), *DNAH11* [MIM 603339], *DNAI1* [MIM 604366], *DNAI2* [MIM 605483], *TXNDC3* [MIM 607421]) that encode dynein-arm components that are responsible for ciliary beat generation.[4–8] In motile cilia, the ciliary axonemes contain nine peripheral doublets, which have attached outer dynein arms (ODAs) and inner dynein arms (IDAs). The beating of each individual cilium is generated by coordinated activation and inactivation of the dynein motor proteins due to ATP-dependent conformational changes of dynein heavy chains.[1] To identify novel genetic PCD variants, we performed total-genome scans by using single-nucleotide polymorphism (SNP) arrays (10K Affymetrix SNP array [Affymetrix, Santa Clara, CA, USA]) in seven consanguineous PCD families with combined ODA and IDA defects. We obtained informed consent from patients and family members enrolled in the study, using protocols approved by the Institutional Ethics Review Board at the University of Freiburg and collaborating institutions. The maximum LOD scores (Zm) were calculated with the ALLEGRO program, with the assumption of autosomal-recessive inheritance with complete penetrance and a calculated disease-allele frequency of 0.0001. In family OP250, we identified four positional candidate-gene regions with a size larger than 10 Mb on chromosomes 10 (26.2 Mb, Zm = 1.33), 11 (16.8 Mb, Zm = 1.33), 16 (10.2 Mb, Zm = 1.33), and 17 (19.4 Mb, Zm = 1.33) (see Figure S1, available online). Haplotype analyses were consistent with homozygosity by descent (data not shown). The positional candidate-gene regions contained a total of ~770 genes. We considered *LRRC50*, located on chromosome 16q24 (Figure 1C), as a strong candidate for PCD, because the reported ultrastructural phenotype of cilia and flagella in zebrafish and *Chlamydomonas* algae carrying mutations in orthologous genes showed defects of ODA and IDA structures.[9–12] The affected 16-year-old patient (OP250-II1) showed similar dynein-arm defects. We therefore decided to analyze *LRRC50* first. Genomic DNA was isolated via standard methods directly from blood samples or from lymphocyte cultures after Epstein-Barr virus transformation. Amplification of 12 genomic fragments comprising all exons of *LRRC50* was performed. Indeed, DNA sequencing of this patient identified a homozygous

[1]Department of Paediatrics and Adolescent Medicine, University Hospital 79106 Freiburg, Germany; [2]Faculty of Biology, Albert-Ludwigs-University, 79104 Freiburg, Germany; [3]Institut für Molekularbiologie, Medizinische Hochschule Hannover, 30625 Hanover, Germany; [4]Department of Pathology, [5]Department of Pediatrics, [6]Department of Medicine, University of North Carolina, Chapel Hill, NC 27599-3380, USA; [7]Department of Tumor Virology, German Cancer Research Center, 69120 Heidelberg, Germany; [8]Zentrum für Neugeborene, Kinder und Jugendliche, Klinikum Nürnberg Süd, 90471 Nürnberg, Germany; [9]Cologne Center for Genomics and Institute for Genetics, 50674 Cologne, Germany; [10]Center for Molecular Medicine Cologne, 50931 Cologne, Germany; [11]Cologne Excellence Cluster on Cellular Stress Responses in Aging-associated Diseases (CECAD), University of Cologne, 50674 Cologne, Germany; [12]Max-Planck Institute for Molecular Genetics, 14195 Berlin, Germany; [13]Klinik und Poliklinik für Kinder- und Jugendmedizin - Allgemeine Pädiatrie - Universitätsklinikum Münster, Albert-Schweitzer-Strasse 33; 48149 Münster, Germany
[14]These authors contributed equally to this work
*Correspondence: heymut.omran@uniklinik-freiburg.de
DOI 10.1016/j.ajhg.2009.10.018.

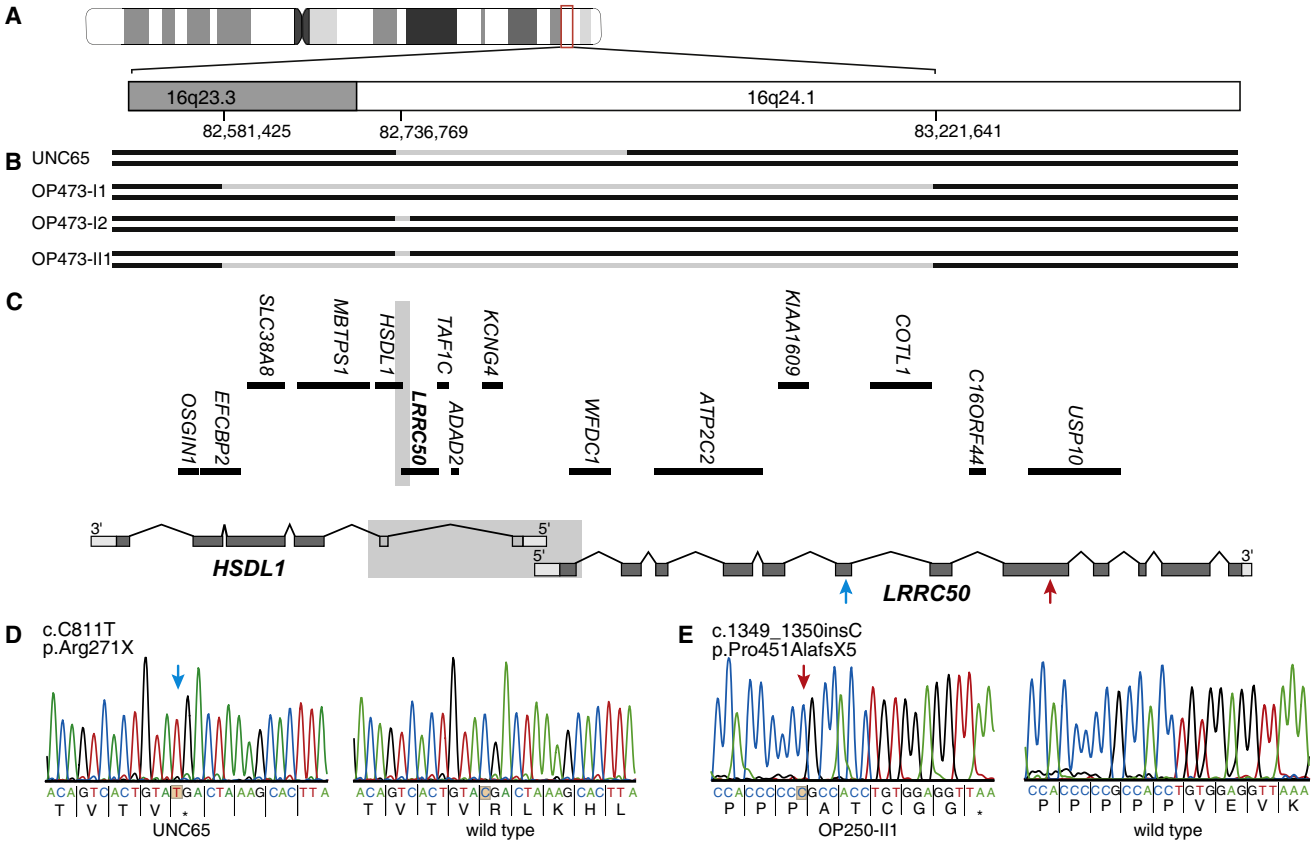

Figure 1. Chromosomal Array and Mutations of *LRRC50*
(A) *LRRC50* is located on 16q24.1.
(B) Chromosomes of four individuals carrying deletions involving LRRC50 are shown. The gray bars mark the deletions.
(C–E) Array of the genes located in the genomic interval of interest; genomic structure of *HSDL1* and *LRRC50* (C). The arrows indicate the position of the detected point mutations shown in (D) (mutation of UNC65) and (E) (mutation of OP250-II1).

loss-of-function mutation (c.1349_1350insC), which predicts a premature stop of translation (p.Pro451AlafsX5) (Figure 1E). Consistent with homozygosity by descent, both parents were heterozygous carriers of the mutation (Figure S2). In the next step, we analyzed 58 additional PCD families with ODA defects for the presence of *LRRC50* mutations. Interestingly, we were unable to perform PCR amplification of exon 1 of *LRRC50* in a 4-year-old child (OP473-II1), consistent with a homozygous deletion. Further PCR amplification showed that the biallelic deletion also involved the first two exons of the adjacent gene *HSDL1*. Additional analyses using high-resolution SNP genotyping and quantitative PCR corroborated this finding (Figures 1B and 1C). The Affymetrix genome-wide Human SNP Array 6.0, utilizing more than 906,600 SNPs, was used for the detection of copy-number variations in four individuals (OP473-I1, OP473-I2, OP473-II1, UNC65) harboring genomic deletions involving *LRRC50*. Quantitative data analysis was performed with GTC 3.0.1 (Affymetrix Genotyping Console) with the use of HapMap270 (Affymetrix) as a reference file. For the performance of quantitative PCR, 50 ng of each DNA sample were amplified in a 25 μl reaction containing 0,1 μmol/l of each primer and 2× Absolute QPCR SYBR GreenMix (Thermo Scientific). Amplification was performed on the Eppendorf realplex2 LightCycler, consisting of a preincubation at 95°C for 15 min, followed by 40 cycles of denaturation at 95°C for 15 s, annealing at 60°C for 30 s, and extension at 72°C for 30 s. Samples were amplified in duplicate for both the target exon and the reference gene (*BRAF*). We demonstrated that the child inherited a small maternal deletion (~11 kb) involving the 5′ ends of *LRRC50* and *HSDL1* and a large paternal deletion (Figures 1B and 1C, Figure 2, Figure S3). The paternal 640 kb deletion involves the genes *EFCBP2*, *SLC38A8*, *MBTPS1* (MIM 603355), *HSDL1*, *LRRC50*, *TAF1C* (MIM 604905), *ADAD2*, *KCNG4* (MIM 607603), *WFDC1* (MIM 605322), *ATP2C2*, *KIAA1609*, and *COTL1* (MIM 606748). Using cross-breakpoint PCR, we identified the exact site of the breakpoints of the smaller deletion (Figure 2, Figure S3). On the basis of sequence comparison, we assume that the deletions originated from multiple-copy repetitive elements (Alu consensus sequences) present in the adjacent genomic regions of the breakpoints, promoting nonhomologous recombinations. In addition, we identified in the U.S. PCD patient UNC65 a nonsense *LRRC50* mutation (c.C811T) predicting premature termination of translation (p.Arg271X; Figure 1D). Because no parental

DNA was available for this deceased individual, we were unable to distinguish by segregation analysis whether this patient carries homozygous point mutations or carries a heterozygous deletion. Using the Affymetrix genome-wide Human SNP Array 6.0, we found that this individual indeed carries a heterozygous deletion of the 5′ untranslated region (UTR) and the first exon of the *LRRC50* gene. Quantitative SNP analyses confirmed the presence of a heterozygous deletion (~220 kb) involving the six genes *HSDL1*, *LRRC50*, *TAF1C*, *ADAD2*, *KCNG4*, and *WFDC1* (Figure 1B).

Thus, we provide evidence that recessive loss-of function point mutations and larger genomic deletions involving *LRRC50* can cause PCD. This is, to our knowledge, the first report that large genomic rearrangements can play a role in the etiology of PCD. Because heterozygous deletions cannot be detected by DNA sequencing of PCR-amplified fragments, this finding must be considered when analyzing the *LRRC50* gene. Interestingly, the larger deletions present in patients UNC65, OP473-I1, and OP473–II1 extend to a genomic region on chromosome 16q24 of frequent loss of heterozygosity (LOH) that has been previously identified in multiple cancers, including prostate, breast, hepatocellular, and Wilms' tumor[13] (MIM 194070). LOH on chromosome 16q is one of the most consistent genetic alterations in sporadic prostate cancer. Elo et al. reported distinct deletions in sporadic prostate cancer involving 16q24.1-q24.2 and 16q24.3-qter.[14] Lange et al. found evidence for linkage at 16q23, but failed to identify a putative hereditary prostate cancer gene at 16q23.[15] Thus, the detection in PCD patients of somatic deletions involving these genomic intervals might be of broader interest, because these individuals might carry an increased risk of developing cancers.

Consistent with a functional role of LRRC50 for determination of left-right asymmetry, in the three individuals carrying recessive loss-of-function *LRRC50* mutations, two of them (OP250-II1 [Figure 3G] and UNC65) exhibit *situs inversus totalis*, and one (OP473-II1) has *situs solitus* (Figure 3H). Thus, the genetic defect causes randomization of left-right body asymmetry as observed in *lrrc50* mutant fish.[11,12] This is probably explained by defective function of motile monocilia located at the node in mammals or the orthologous structure (Kupffer's vesicle) in zebrafish during embryogenesis, because it was previously shown that a "nodal flow" produced by those cilia is essential for determination of left-right asymmetry.[2,16] Consistent with a role for nodal ciliary motion, *lrrc50* expression was reported in the Kupffer's vesicle.[17] To visualize gene expression on the cellular level in mouse embryos, we used a 1260 bp probe comprising mainly the 3′ UTR of *Lrrc50* (NC_000074.5) to perform in situ hybridization analysis of whole mouse embryos (7.5 days postcoitum [dpc] to 11.5 dpc) and embryonic (14.5 dpc and 16.5 dpc) and adult kidney sections, as described previously.[4] As expected we found expression of the mouse ortholog *Lrrc50* at the node via in situ hybridization (stages E7.75 and E8.0; Figures 3B and 3C). PCD patients suffered from chronic upper- and lower-airway infections due to reduced mucociliary clearance of the respiratory tract. At the age of 16 years, patient OP250-II1 showed severe bronchiectasis. Because of destructive lung disease in patient UNC65, a partial lobectomy of the left lung was performed at age 25. Consistent with a role of LRRC50 for ciliary motility in respiratory cells, we found specific *Lrrc50* expression in ciliated mouse respiratory cells (stage E16.5; Figures 3E and 3F). Two of the affected individuals were available for functional analyses of the respiratory ciliary beating. High-speed videomicroscopy evaluation of the ciliary beating pattern with the SAVA system revealed immotile cilia in both individuals (Movies S1–S3), highlighting the importance of LRRC50 for cilia beat generation. Transmission electron microscopy of respiratory ciliary axonemes showed a marked reduction of both ODAs and IDAs (Figure 4A), which appeared to be more severe than findings previously described in PCD patients with *KTU* (MIM 612517) mutations.[18] To gain further insight into the functional role of LRRC50, we performed high-resolution immunofluorescence microscopy in control and *LRRC50* mutant respiratory cells from patients Op473-II1 and Op250-II1, using specific antibodies directed against various dynein-arm components (Figures 4B–4E) as described previously.[18] Anti-DNAH5 and anti-DNAI2 target two distinct ODA subtypes. Anti-DNAH9 stains only the distally located (type 2) ODA complexes. We observed complete absence of the ODA heavy chains DNAH5 and DNAH9 (MIM 603330) and the ODA intermediate chain DNAI2 from the ciliary axonemes, indicating that loss of LRRC50 affects the assembly of proximally (type 1) and distally (type 2) located ODA complexes in respiratory cells.[18,19] Analyses of DNALI1 (an ortholog of *Chlamydomonas reinhardtii* IDA light chain p28) revealed that this IDA component was also absent from all mutant ciliary axonemes and instead accumulated in the cytoplasm. Hence, in LRRC50 mutant cilia of patients OP250-II1 (Figure 2) and OP473 (not shown), combined ODA and IDA defects are present. The only other known PCD variant exhibiting combined ODA and IDA defects is caused by recessive *KTU* mutations that disrupt cytoplasmic preassembly of dynein-arm complexes.[18] The defects observed in *LRRC50* mutant cells are more severe than those in *KTU* mutant cells because in those cilia, some ODA proteins, such as DNAH5 and DNAI2, can still be assembled in the proximal cilium. The presence of a combined ODA and IDA defect in patients with *LRRC50* mutations parallels findings obtained in *Chlamydomonas* algae carrying orthologous mutations.[10] We assume that LRRC50 as shown for KTU plays a role in cytoplasmic preassembly and/or targeting of dynein-arm complexes.[18] Consistent with such an explanation, DNALI1 is still detectable in the cytoplasm.

Interestingly, on the basis of previous studies in *lrrc50* mutant zebrafish and mammalian renal cell lines, it has been suggested that LRRC50 plays a role in human cystic

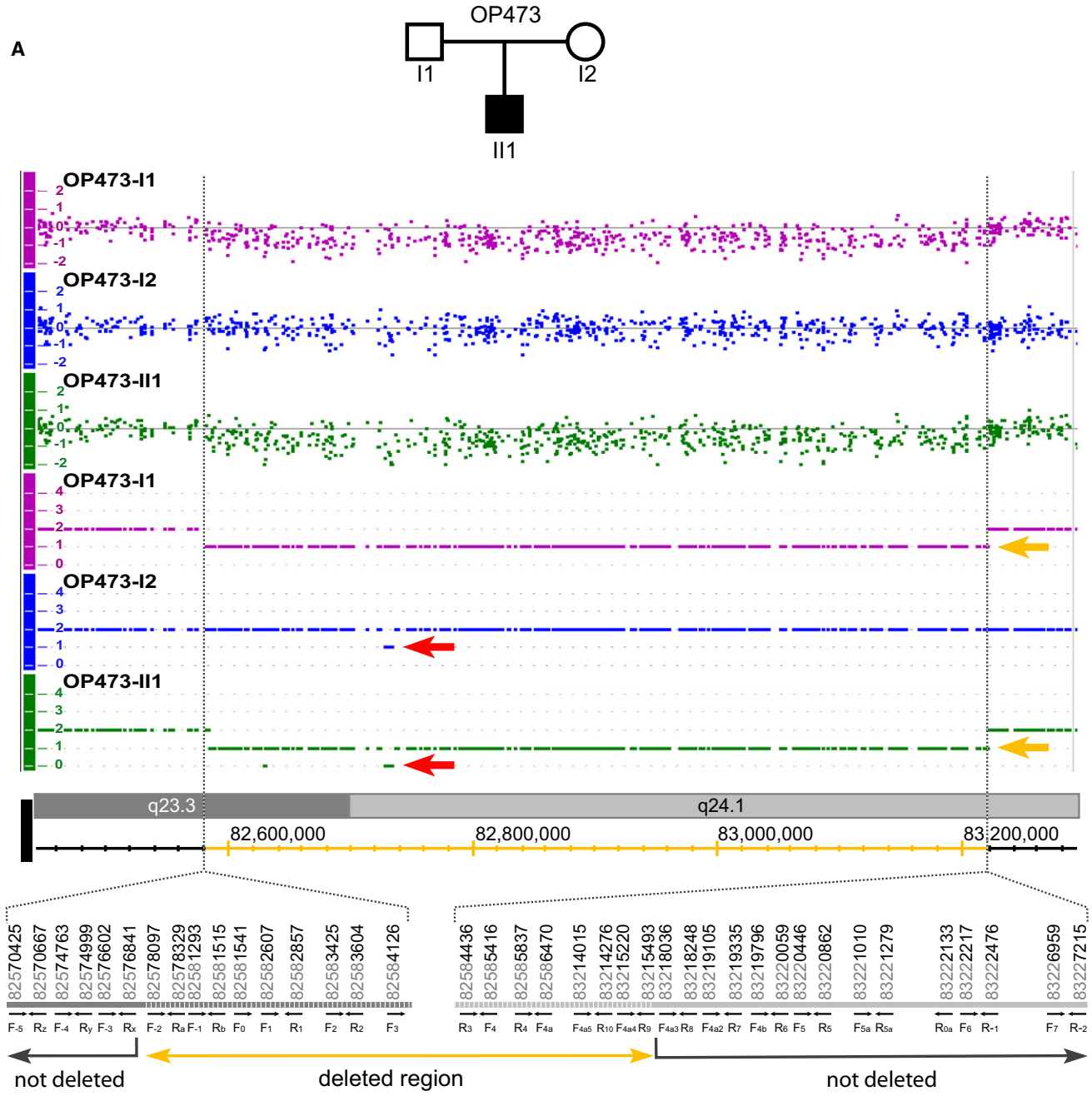
A
OP473
I1
I2
II1
OP473-I1
OP473-I2
OP473-II1
OP473-I1
OP473-I2
OP473-II1
q23.3
q24.1
82,600,000
82,800,000
83,000,000
83,200,000
82570425 82570667 82574763 82574999 82576602 82576841 82578097 82578329 82581293 82581515 82581541 82582607 82582857 82583425 82583604 82584126
F-5 Rz F-4 Ry F-3 Rx F-2 Ra F-1 Rb F0 F1 R1 F2 R2 F3
82584436 82585416 82585837 82586470 83214015 83214276 83215220 83215493 83218036 83218248 83219105 83219335 83219796 83220059 83220446 83220862 83221010 83221279 83222133 83222217 83222476 83226959 83227215
R3 F4 R4 F4a F4a5 R10 F4a4 R9 F4a3 R8 F4a2 R7 F4b R6 F5 R5 F5a R5a R0a F6 R-1 F7 R-2
not deleted
deleted region
not deleted
B
UNC65
UNC65
q23.3
q24.1
82,600,000
82,800,000
83,000,000
83,200,000

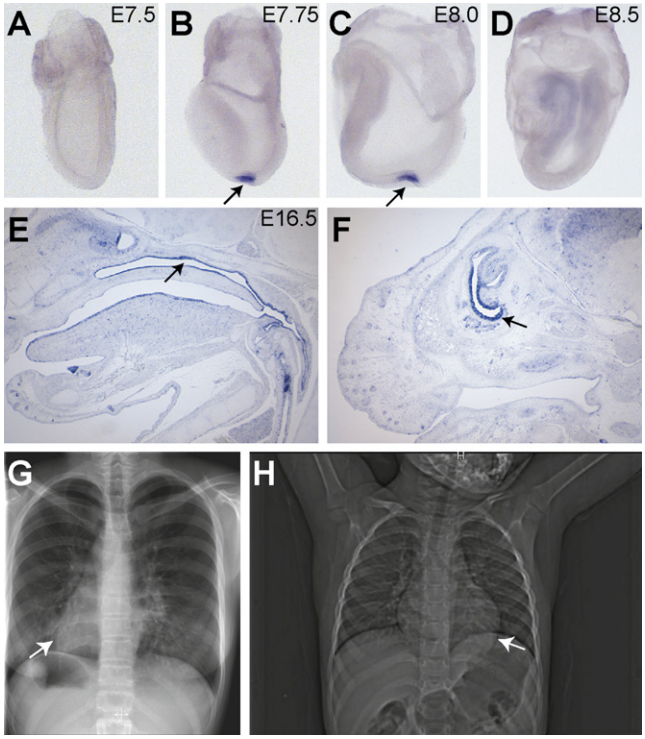

Figure 3. Expression of Mouse *Lrrc50* and Randomization of Left-Right Body Asymmetry in Patients with *LRRC50* Mutations
(A–D) Whole-mount in situ hybridization analysis of mouse *Lrrc50* in early gastrulation-stage embryos. *Lrrc50* expression is restricted to the node in embryos at 7.75–8.0 dpc (B and C; arrow).
(E and F) *Lrrc50* expression (arrow) in ciliated cells of the upper airways in 16.5 dpc mouse embryonic sections. (E). Midline sagittal section; arrow depicts nasopharynx. (F) Parasagittal section; arrow depicts respiratory epithelium of the nasal cavity. The identical probe is used in all in situ hybridization panels.
(G) Patient OP250-II1 has *situs inversus totalis* and patient OP473-II1 has *situs solitus*.
(H) The hearts are marked by arrows. Thus, mutations of *LRRC50* cause randomization of left-right body asymmetry.

kidney disease.[12] Therefore, we checked whether individuals with recessive loss-of-function *LRRC50* mutations developed cystic kidney disease. Interestingly, in all patients, including the 55-year-old UNC65 patient, no renal disease was present. Lack of *Lrrc50* expression in mouse embryonic and adult kidneys (data not shown) also supports that in humans and mice *LRRC50*/*Lrrc50* probably has no functional role in the kidneys. This may reflect a difference in the functional role of motile cilia for mesonephric (fish) and metanephric (mouse and man) kidneys.

We detected *LRRC50* mutations in three of 59 PCD families (~5%) with dynein-arm defects. In most of these families, other genetic defects, such as *DNAH5* mutations, had been already excluded. Because combined ODA and IDA defects are very rare and *LRRC50* mutations contribute to only a portion of those defects, the overall frequency of *LRRC50* mutations in the PCD population is probably very low.

Supplemental Data

Supplemental Data include three figures and three movies and can be found with this article online at http://www.cell.com/AJHG.

Acknowledgments

We are grateful to the patients and their families for their participation in this study. We thank the German patient support group Kartagener Syndrom und Primaere Ciliaere Dyskinesie e.V. and the U.S. PCD Foundation. We thank Carmen Kopp, Karin Sutter, Marianne Petry, Christian Kluck, Claudia Tessmer, Theresia de Ledezma, and Susanne Franz for excellent technical assistance. We also thank Peadar Noone, Marcus Kennedy, Johnny Carson, Milan Hazucha, Susan Minnix, Kim Burns, Lucy Morgan, Robbert De Iongand, Sharon Dell, and Tom Ferkol for evaluation of PCD patients. This work was supported by grants from the Deutsche Forschungsgemeinschaft (DFG) (Om 6/4, GRK1104, BIOSS, and SFB592; to H.O.), grants from the U.S. National Heart, Lung and Blood Institute and the National Institutes of Health (NIH) (GCRC 00046 and R01 HL071798), and a grant from the 5 U54 RR019480 from the U.S. National Center for Research Resources and the NIH (to M.R.K.).

Received: August 26, 2009
Revised: October 14, 2009
Accepted: October 21, 2009
Published online: November 25, 2009

Web Resources

The URL for data presented herein is as follows:

Online Mendelian Inheritance in Man (OMIM), http://www.ncbi.nlm.nih.gov/Omim/

References

1. Fliegauf, M., Benzing, T., and Omran, H. (2007). When cilia go bad: cilia defects and ciliopathies. Nat. Rev. Mol. Cell Biol. *8*, 880–893.

Figure 2. Deletions on the Alleles of Family OP473 and Patient UNC65
(A) Results of quantitative SNP analysis from the parents of the affected child with PCD (OP473-II1). The graphs indicate log2ratio and copy-number state as a function of genomic position. The father (OP473-I1) carries a large (~640 kb) deletion on one allele (marked by a yellow arrow), and the mother (OP473-I2) carries a small (11 kb) deletion on one allele (marked by a red arrow) within the region of *HSDL1* and *LRRC50*. The affected son inherited both deleted alleles. The mother's deleted block contained six SNPs and two copy-number variants. Lower panel: The positions of the first 5′ base of primers used for quantitative PCR are given. The breakpoints of the larger deletion are located between primers Rx and Ra (distance: 1488 bp) on 16q23.3 and primers F4a4 and F4a3 (distance: 2816 bp) on 16q24.1. We were unable to narrow this region further because of repetitive Alu elements present within these regions.
(B) Patient UNC65 carries a ~220 kb deletion on one allele (marked by a blue arrow). On the other allele, a point mutation (Figure 1D) was identified.

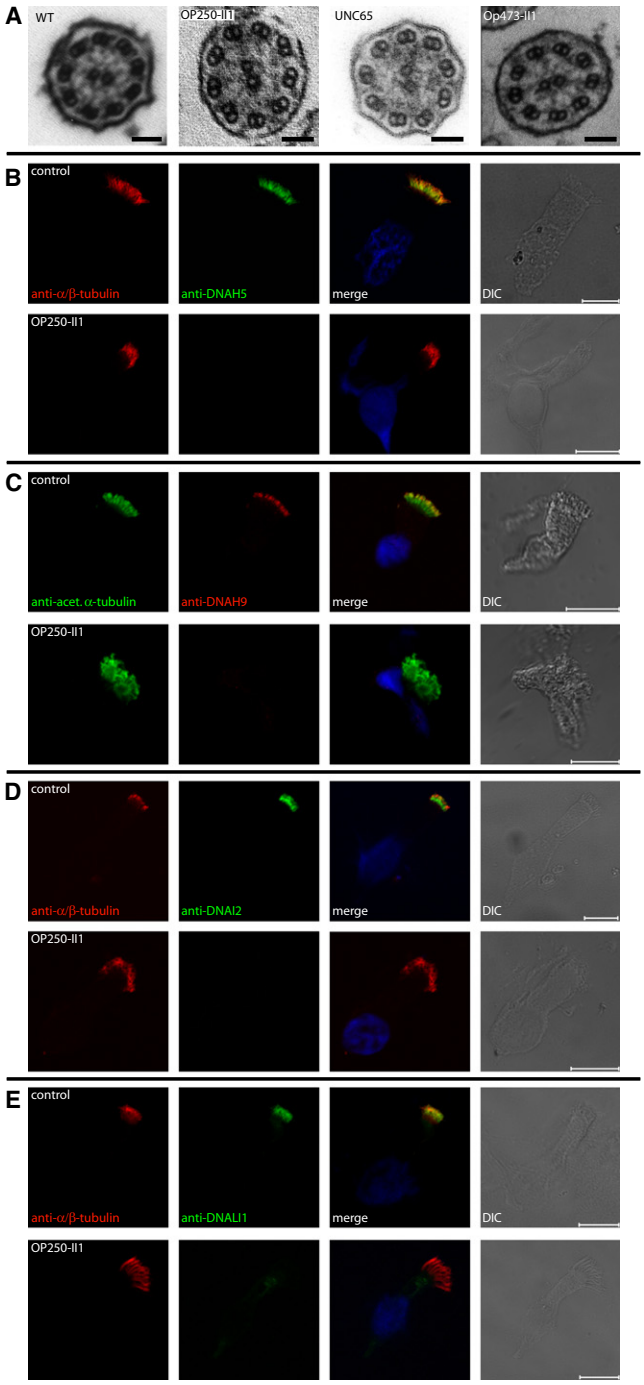

Figure 4. Axonemal Defects of the IDA and ODA in PCD Patients with *LRRC50* Mutations

(A) Transmission electron micrographs of cross-sections from respiratory cilia from patients OP250-II1, UNC65, and OP473-II1. Please note ODA and IDA defects as compared to an electron micrograph from a healthy control.

(B–E) High-resolution immunofluorescence microscopy of respiratory cells from a healthy control and patient OP250-II1 with the use of specific antibodies directed against ODA chains DNAH5 (B), DNAH9 (C), DNAI2 (D), and IDA component DNALI1 (E). Acetylated α-tubulin and α/β-tubulin were stained as control for ciliary axonemes. In LRRC50 mutant respiratory cells, outer dynein chains DNAH5 (B), DNAH9 (C), and DNAI2 (D) are completely absent from the axonemes of mutant respiratory cells. The inner dynein chain DNALI1 is also completely absent from mutant ciliary axonemes (E). Nuclei were stained with Hoechst 33342 (blue). Black scale bars (A) represent 0.1 μm and white scale bars (B–E) represent 10 μm.

2. Nonaka, S., Tanaka, Y., Okada, Y., Takeda, S., Harada, A., Kanai, Y., Kido, M., and Hirokawa, N. (1998). Randomization of left-right asymmetry due to loss of nodal cilia generating leftward flow of extraembryonic fluid in mice lacking KIF3B motor protein. Cell *95*, 829–837.
3. Ibanez-Tallon, I., Pagenstecher, A., Fliegauf, M., Olbrich, H., Kispert, A., Ketelsen, U.P., North, A., Heintz, N., and Omran, H. (2004). Dysfunction of axonemal dynein heavy chain Mdnah5 inhibits ependymal flow and reveals a novel mechanism for hydrocephalus formation. Hum. Mol. Genet. *13*, 2133–2141.
4. Olbrich, H., Häffner, K., Kispert, A., Völkel, A., Volz, A., Sasmaz, G., Reinhardt, R., Hennig, S., Lehrach, H., Konietzko, N., et al. (2002). Mutations in DNAH5 cause primary ciliary dyskinesia and randomization of left-right asymmetry. Nat. Genet. *30*, 143–144.
5. Schwabe, G.C., Hoffmann, K., Loges, N.T., Birker, D., Rossier, C., de Santi, M.M., Olbrich, H., Fliegauf, M., Failly, M., Liebers, U., et al. (2008). Primary ciliary dyskinesia associated with normal axoneme ultrastructure is caused by DNAH11 mutations. Hum. Mutat. *29*, 289–298.
6. Pennarun, G., Escudier, E., Chapelin, C., Bridoux, A.M., Cacheux, V., Roger, G., Clément, A., Goossens, M., Amselem, S., and Duriez, B. (1999). Loss-of-function mutations in a human gene related to Chlamydomonas reinhardtii dynein IC78 result in primary ciliary dyskinesia. Am. J. Hum. Genet. *65*, 1508–1519.
7. Loges, N.T., Olbrich, H., Fenske, L., Mussaffi, H., Horvath, J., Fliegauf, M., Kuhl, H., Baktai, G., Peterffy, E., Chodhari, R., et al. (2008). DNAI2 mutations cause primary ciliary dyskinesia with defects in the outer dynein arm. Am. J. Hum. Genet. *83*, 547–558.
8. Duriez, B., Duquesnoy, P., Escudier, E., Bridoux, A.M., Escalier, D., Rayet, I., Marcos, E., Vojtek, A.M., Bercher, J.F., and Amselem, S. (2007). A common variant in combination with a nonsense mutation in a member of the thioredoxin family causes primary ciliary dyskinesia. Proc. Natl. Acad. Sci. USA *104*, 3336–3341.
9. Fowkes, M.E., and Mitchell, D.R. (1998). The role of preassembled cytoplasmic complexes in assembly of flagellar dynein subunits. Mol. Biol. Cell *9*, 2337–2347.
10. Freshour, J., Yokoyama, R., and Mitchell, D.R. (2007). Chlamydomonas flagellar outer row dynein assembly protein ODA7 interacts with both outer row and I1 inner row dyneins. J. Biol. Chem. *282*, 5404–5412.
11. Sullivan-Brown, J., Schottenfeld, J., Okabe, N., Hostetter, C.L., Serluca, F.C., Thiberge, S.Y., and Burdine, R.D. (2008). Zebrafish mutations affecting cilia motility share similar cystic phenotypes and suggest a mechanism of cyst formation that differs from pkd2 morphants. Dev. Biol. *314*, 261–275.
12. Van Rooijen, E., Giles, R.H., Voest, E.E., van Rooijen, C., Schulte-Merker, S., and van Eeden, F.J. (2008). LRRC50, a conserved ciliary protein implicated in polycystic kidney disease. J. Am. Soc. Nephrol. *19*, 1128–1138.
13. Larsen, M., Ressler, S.J., Gerdes, M.J., Lu, B., Byron, M., Lawrence, J.B., and Rowley, D.R. (2000). The WFDC1 gene encoding ps20 localizes to 16q24, a region of LOH in multiple cancers. Mamm. Genome *11*, 767–773.

14. Elo, J.P., Härkönen, P., Kyllönen, A.P., Lukkarinen, O., and Vihko, P. (1999). Three independently deleted regions at chromosome arm 16q in human prostate cancer: allelic loss at 16q24.1-q24.2 is associated with aggressive behaviour of the disease, recurrent growth, poor differentiation of the tumour and poor prognosis for the patient. Br. J. Cancer *79*, 156–160.
15. Lange, E.M., Beebe-Dimmer, J.L., Ray, A.M., Zuhlke, K.A., Ellis, J., Wang, Y., Walters, S., and Cooney, K.A. (2009). Genome-wide linkage scan for prostate cancer susceptibility from the University of Michigan Prostate Cancer Genetics Project: suggestive evidence for linkage at 16q23. Prostate *69*, 385–391.
16. Kramer-Zucker, A.G., Olale, F., Haycraft, C.J., Yoder, B.K., Schier, A.F., and Drummond, I.A. (2005). Cilia-driven fluid flow in the zebrafish pronephros, brain and Kupffer's vesicle is required for normal organogenesis. Development *132*, 1907–1921.
17. Essner, J.J., Amack, J.D., Nyholm, M.K., Harris, E.B., and Yost, H.J. (2005). Kupffer's vesicle is a ciliated organ of asymmetry in the zebrafish embryo that initiates left-right development of the brain, heart and gut. Development *132*, 1247–1260.
18. Omran, H., Kobayashi, D., Olbrich, H., Tsukahara, T., Loges, N.T., Hagiwara, H., Zhang, Q., Leblond, G., O'Toole, E., Hara, C., et al. (2008). Ktu/PF13 is required for cytoplasmic pre-assembly of axonemal dyneins. Nature *456*, 611–616.
19. Fliegauf, M., Olbrich, H., Horvath, J., Wildhaber, J.H., Zariwala, M.A., Kennedy, M., Knowles, M.R., and Omran, H. (2005). Mislocalization of DNAH5 and DNAH9 in respiratory cells from patients with primary ciliary dyskinesia. Am. J. Respir. Crit. Care Med. *171*, 1343–1349.